JCB Journal of Cell Biology

ARTICLE

β-Catenin is a pH sensor with decreased stability at higher intracellular pH

Katharine A. White[1*], Bree K. Grillo-Hill[2*], Mario Esquivel[1], Jobelle Peralta[2], Vivian N. Bui[2], Ismahan Chire[2], and Diane L. Barber[1]

β-Catenin functions as an adherens junction protein for cell–cell adhesion and as a signaling protein. β-catenin function is dependent on its stability, which is regulated by protein–protein interactions that stabilize β-catenin or target it for proteasome-mediated degradation. In this study, we show that β-catenin stability is regulated by intracellular pH (pHi) dynamics, with decreased stability at higher pHi in both mammalian cells and *Drosophila melanogaster*. β-Catenin degradation requires phosphorylation of N-terminal residues for recognition by the E3 ligase β-TrCP. While β-catenin phosphorylation was pH independent, higher pHi induced increased β-TrCP binding and decreased β-catenin stability. An evolutionarily conserved histidine in β-catenin (found in the β-TrCP DSGIHS destruction motif) is required for pH-dependent binding to β-TrCP. Expressing a cancer-associated H36R–β-catenin mutant in the *Drosophila* eye was sufficient to induce Wnt signaling and produced pronounced tumors not seen with other oncogenic β-catenin alleles. We identify pHi dynamics as a previously unrecognized regulator of β-catenin stability, functioning in coincidence with phosphorylation.

Introduction

β-Catenin functions as both an adherens junction protein for cell–cell adhesion and a signaling molecule for canonical Wnt signaling (Valenta et al., 2012). β-Catenin is essential for growth, differentiation, and cell polarity, and increased β-catenin protein levels, usually achieved by mutation, correlate with pathological progression in epithelial carcinomas (Klaus and Birchmeier, 2008). β-Catenin abundance is predominantly regulated by obligatory phosphorylation of N-terminal residues followed by ubiquitination and proteasome-mediated degradation (Aberle et al., 1997; Daugherty and Gottardi, 2007), although lysosome-mediated degradation (Petherick et al., 2013) and exosome-mediated release (Chairoungdua et al., 2010) have also been reported. The importance of proteasome-mediated degradation in regulating β-catenin function is reflected in cancer-associated mutations that prevent or block proteasome-mediated degradation, resulting in enhanced tumorigenesis (Morin et al., 1997; Peifer and Polakis, 2000).

Proteasome-mediated degradation of β-catenin requires the N-terminal regulatory region (residues 1–133) with obligate phosphorylation of one serine by the priming kinase casein kinase 1 (CK1) followed by processive phosphorylation of two serines and one threonine by glycogen synthase kinase-3β (GSK3β; Liu et al., 2002; Sadot et al., 2002). The E3 ligase β-TrCP recognizes β-catenin at these phosphorylated residues and ubiquitinates β-catenin, targeting it for proteasome-mediated degradation. Mutations in conserved phosphorylated residues Ser33/37 and Thr41 increase β-catenin abundance and correlate with pathological progression in lung (Li et al., 2013), colorectal (Morin et al., 1997), and hepatocellular (Endo et al., 2000) carcinomas. The current view is that phosphorylation of β-catenin by GSK3β at just two residues (Ser33 and Ser37) is both necessary and sufficient for β-TrCP association (Aberle et al., 1997; Ha et al., 2004).

In this study, we report that β-catenin abundance and stability are also regulated by intracellular pH (pHi) dynamics, with increased β-TrCP binding and decreased stability at higher pHi. While β-catenin phosphorylation by both CK1 and GSK3β are unaffected by pHi, an evolutionarily conserved histidine (His36 in human β-catenin) in the β-TrCP binding motif (DSGIHS) mediates pH-sensitive association with β-TrCP. Our data identify pHi dynamics as a previously unrecognized regulator of β-catenin stability, which functions in coincidence with phosphorylation.

Results

We previously reported that overexpression of *DNhe2*, an orthologue of the mammalian Na–H exchanger NHE1, in the developing *Drosophila melanogaster* eye increases pHi from 7.3 to 7.7 and is sufficient to induce a rough eye phenotype with underlying dysplasia in the absence of an activated oncogene (Grillo-Hill et al., 2015). To identify potential mediators of the

[1]Department of Cell and Tissue Biology, University of California, San Francisco, San Francisco, CA; [2]Department of Biological Sciences, San Jose State University, San Jose, CA.

*K.A. White and B.K. Grillo-Hill contributed equally to this paper; Correspondence to Diane L. Barber: diane.barber@ucsf.edu; Bree K. Grillo-Hill: bree.grillo-hill@sjsu.edu.

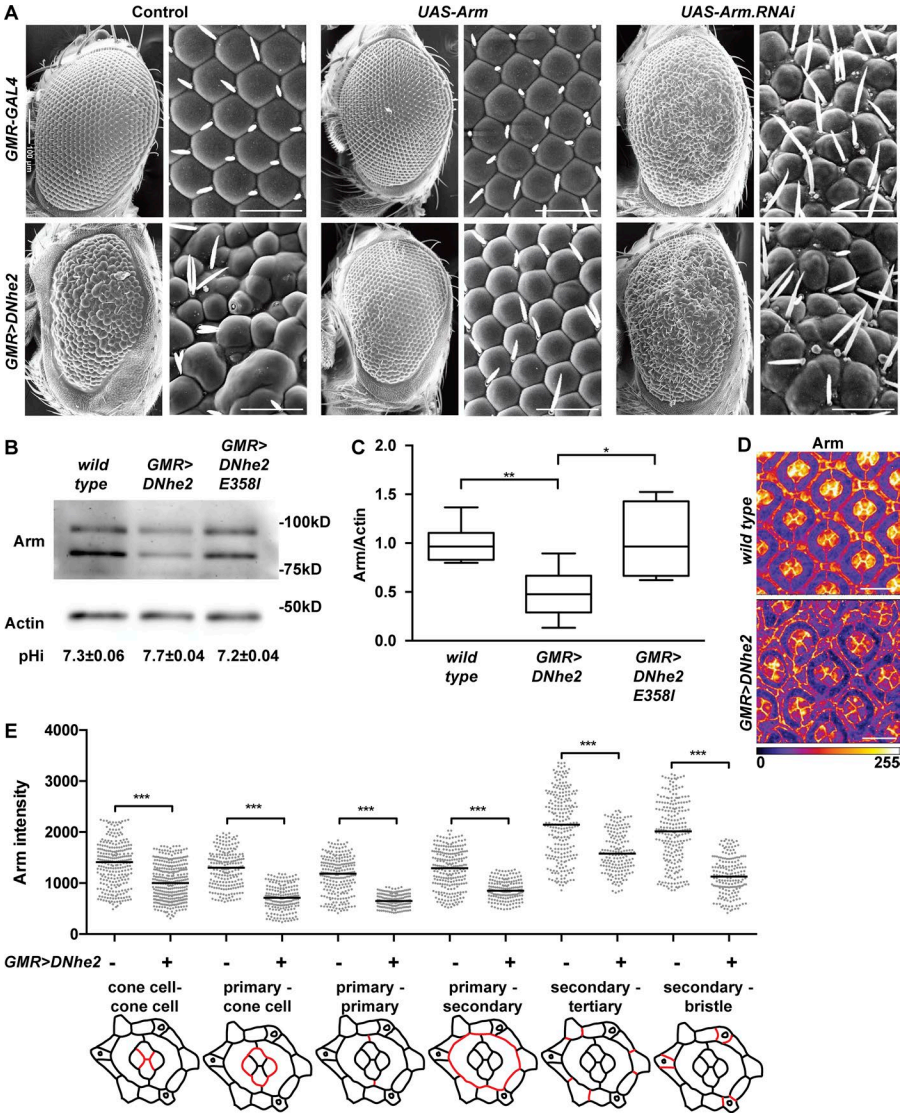

Figure 1. **Overexpression of DNhe2 decreases Arm abundance. (A)** Scanning electron micrographs of adult *Drosophila* eyes depicting genetic interactions between control (*GMR-GAL4*) and overexpression of *DNhe2* (*GMR>DNhe2*) with overexpression of *arm* (*UAS-Arm*) and RNAi-mediated knockdown of Arm (*UAS-Arm.RNAi4*). Bars, 25 µm. **(B)** Representative immunoblots of Arm and actin from adult *Drosophila* head lysates obtained from three *Drosophila* lines: *WT*, *GMR>DNhe2*, and overexpression of a transporter-dead *DNhe2* mutant (*GMR>DNhe2^{E358I}*). **(C)** Quantification of immunoblots performed as in B with Arm normalized to actin within each replicate. *WT* and *GMR>DNhe2*, N = 8; *GMR>DNhe2^{E358I}*, N = 4. **(D)** Confocal micrographs of mid-pupal retinae from *WT* or *GMR>DNhe2* flies labeled for Arm pseudocolored to show pixel intensities. Bars, 10 µm. **(E)** Quantitative measurements of fluorescence intensity (in AU) of Arm at adherens junctions in pupal retinae (medians shown). Labeled schematics show which cell junctions (labeled in red) were measured. *N* = 5–7 individual flies per condition; *n* = 164–334 junctions per condition. In C, Tukey boxplots are shown, and significance was determined using an unpaired, two-tailed Student's *t* test with Holm-Sidak's multiple comparisons correction. In E, medians are shown, and significance was determined using the Mann–Whitney test. *, P < 0.05; **, P < 0.01; ***, P < 0.001.

dysplasia phenotype, we performed a dominant modifier screen that revealed a strong genetic interaction between *armadillo (arm)*, the *Drosophila* β-catenin homologue, and overexpression of *DNhe2* under the *GMR-GAL4* driver (*GMR>DNhe2*). Overexpression of *arm* alone had minimal effects on retinal patterning, causing occasionally misplaced bristles (Fig. 1 A) but suppressed the *DNhe2*-induced rough eye. Overexpression of *arm* with *DNhe2* restored the hexagonal shape and arrangement of orderly rows of ommatidia (Fig. 1 A). We also found that RNAi-mediated knockdown of *arm* caused a mild rough eye phenotype with a slightly overgrown appearance (Figs. 1 A and S1 A). This phenotype was enhanced with coexpression of *DNhe2* such that eyes were markedly overgrown and showed distinct black granules resembling necrotic granules. These genetic interactions suggest that the rough eye phenotype seen with *DNhe2* overexpression may be dependent on decreased Arm protein abundance.

We confirmed decreased Arm abundance with increased pHi by immunoblotting adult *Drosophila* whole-head lysates. Compared with WT flies, we found lower levels of endogenous Arm with overexpression of *DNhe2* but not with a transport-inactive mutant *DNhe2^{E358I}*, which does not change pHi or induce a rough eye phenotype (Fig. 1, B and C; Grillo-Hill et al., 2015). These findings suggest that decreased Arm abundance with *DNhe2* overexpression is due to the increased pHi and not to scaffolding functions that are retained by the inactive mutant (Denker et al., 2000; Baumgartner et al., 2004). In addition to decreased total Arm abundance, we observed reduced Arm fluorescence intensity at adherens junctions in *GMR>DNhe2* eyes compared with control (Fig. 1, D and E).

We next asked whether another adherens junctions protein can rescue the *GMR>DNhe2* phenotype. We overexpressed two different transgenes encoding *shotgun* (*shg*), the *Drosophila* homologue of E-cadherin, but neither showed a genetic interaction with *DNhe2* overexpression (Fig. S1 B). Consistent with these results, we also observed no difference in the abundance of endogenous Shg or N-cadherin (CadN) across genotypes (Fig. S1, C and D). These data suggest that increased pHi specifically reduces the abundance of Arm instead of reducing the total abundance of adherens junctions proteins in general.

In *Drosophila* pupal eyes, cadherins are localized to specific cell–cell junctions, with CadN exclusively at cone cell–cone cell

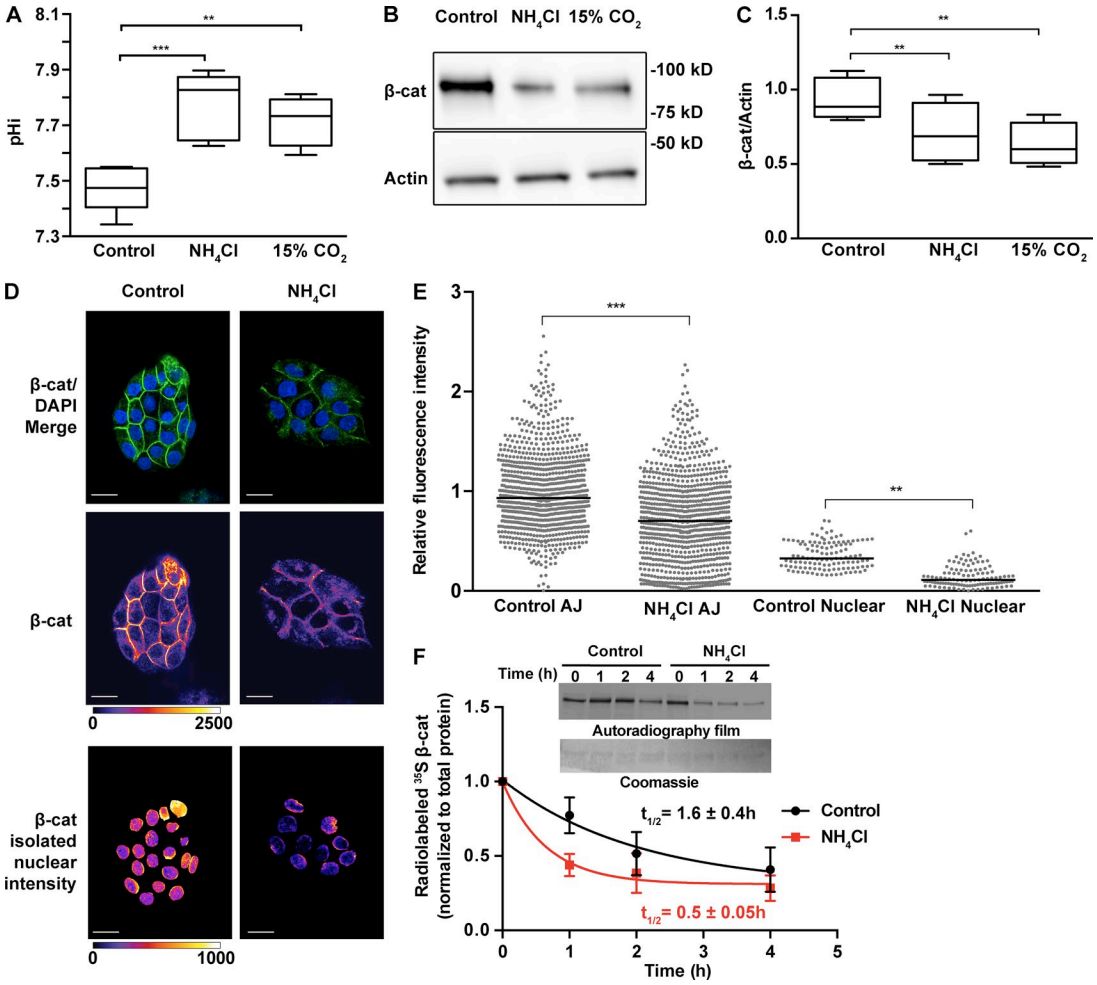

Figure 2. **Higher pHi decreases β-catenin protein levels and stability in MDCK cells. (A)** The pHi of MDCK cells was increased by treating with 5 mM NH_4Cl for 24 h or by maintaining at 15% CO_2 for two passages compared with control untreated cells. **(B)** Representative immunoblots showing total protein levels for β-catenin from cells maintained as in A. **(C)** Quantitative analysis of replicate immunoblots performed as described in B with β-catenin intensity normalized to actin for each replicate. Control and NH_4Cl, N = 6; 15% CO_2, N = 4. **(D)** Confocal images of MDCK cells maintained as in A and fixed and immunolabeled for β-catenin (green), shown merged with DAPI-stained nuclei (blue). Bottom images are pseudocolored to show β-catenin fluorescence intensities of whole-cell and isolated nuclear signals. Bars, 20 µm. **(E)** Quantitative measurements of β-catenin fluorescence intensity at adherens junctions (AJs) and nuclei under conditions described in A. Data were normalized to the mean fluorescence intensity in control cells for each replicate. Adherens junctions: *N* = 7, *n* = 909–962 junctions; nucleus: *N* = 2, *n* = 116–121 nuclei. **(F)** ^{35}S metabolic labeling of β-catenin shows higher rates of protein turnover when pH is increased to 7.8 with 5 mM NH_4Cl. In A and C, Tukey boxplots are shown, and significance was determined using an unpaired, two-tailed Student's *t* test with Holm-Sidak's multiple comparisons correction. In E, medians are shown, and significance was determined using the Mann–Whitney test. **, P < 0.01; ***, P < 0.001.

contacts and Shg at all other cell–cell contacts. In *GMR>DNhe2* pupal eyes, CadN was significantly decreased at cone cell–cone cell contacts (Fig. S1, E and F). However, Shg was significantly decreased at cone cell–primary, primary–primary, and secondary–bristle contacts but not at primary–secondary or secondary–tertiary contacts (Fig. S2, G and H). The contrast with total head lysates, which showed no decrease in Shg or CadN, suggests that changes in junctional localization are independent of total Shg and CadN levels. Taken together, these results indicate that with increased pHi, junctional levels of Arm are reduced across all junctions measured, but effects on junctional cadherin levels are dependent on cell type. The decrease in Arm protein at junctions and in total head lysates suggests a strong and specific pH-sensitive effect on Arm abundance.

Increasing pHi in mammalian cells also reduced β-catenin abundance. We used two methods to increase steady-state pHi in MDCK epithelial cells. Using one previously described approach (White et al., 2017a), we incubated MDCK cells for 24 h with 5 mM NH_4Cl, which increased pHi from 7.4 to 7.8 (Fig. 2 A). Using another approach (Choi et al., 2013), we maintained MDCK cells for 10 d in 15% CO_2, which changes cellular buffering and increased pHi to 7.7 (Fig. 2 A). With both approaches, there was decreased abundance of β-catenin in whole-cell lysates with increased pHi (Fig. 2, B and C). Increasing pHi also decreased β-catenin abundance in mouse mammary NMuMG epithelial cells (Fig. S2, A–C). Additionally, increasing pHi in MDCK cells with NH_4Cl decreased β-catenin abundance at cell–cell junctions and in the nucleus (Fig. 2, D and E). Increasing pHi with 15% CO_2 also decreased β-catenin abundance at junctions but increased the number of double-nucleated cells, suggesting possible cytokinesis defects using this method of pHi control (Fig. S2, D and E). For this reason, we used 5 mM NH_4Cl to increase pHi in all future experiments.

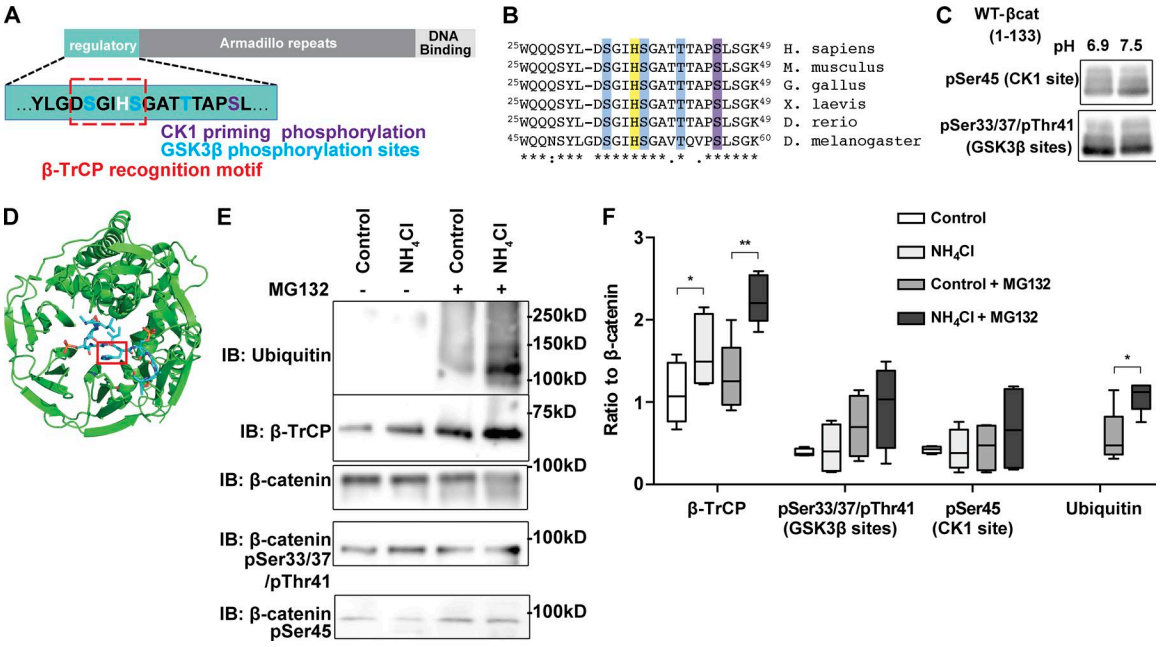

Figure 3. **Higher pHi increases association of β-catenin with the E3 ligase β-TrCP in MDCK cells. (A)** Schematic of β-catenin protein structure. N-terminal residues essential for protein level regulation including Ser45 (purple), which is phosphorylated by CK1, and Ser33/Ser37/Thr41 (blue), which are phosphorylated by GSK3β. Shown in the red box is the β-catenin DSGIHS destruction motif that directly binds to the E3 ligase β-TrCP. **(B)** Sequence alignment of β-catenin orthologues. Indicated are the conserved CK1 (purple) and GSK3β phosphorylation (blue) sites as well as the evolutionarily conserved histidine residue (yellow). **(C)** Truncated β-catenin protein (residues 1–133) was expressed as a fusion to GST and phosphorylated in vitro with CK1 and GSK3β in buffers at pH 6.9 or 7.5 (see Materials and methods for details), with immunoblots showing the extent of pSer45 and pSer33/37/pThr41 at both buffer pH values. **(D)** Structure of β-catenin peptide (residues 29–40; blue stick) complexed with β-TrCP (green cartoon). His36 of β-catenin is highlighted in the red box. PDB: 1P22. **(E)** Representative immunoblots (IBs) of immune complex components following IP of endogenous β-catenin from MDCK cells untreated (control) or treated with 5 mM NH_4Cl for 24 h in the absence and presence of proteasome inhibitor MG132 (see Materials and methods for details). Levels of β-TrCP, phosphorylated β-catenin, and ubiquitinated β-catenin in immune complexes are shown. Equal amounts of immunoprecipitated β-catenin protein were loaded in each well. **(F)** Quantitative analysis of immunoblots as described in E. N = 4. Tukey boxplots are shown, and significance was determined using an unpaired, two-tailed Student's *t* test with Holm-Sidak's multiple comparisons correction. *, P < 0.05; **, P < 0.01.

To test whether pHi effects in MDCK are limited to β-catenin or affect other junctional proteins, we measured total E-cadherin levels by immunoblotting, which were unchanged with increased pHi (Fig. S2, F and G). However, we observed a significant increase in E-cadherin localization at cell–cell junctions with increased pHi in MDCK cells (Fig. S2, H and I). Therefore, while we observed differential effects of increased pHi on cadherin localization in *Drosophila* and mammalian models, Arm/β-catenin reduction at junctions and in whole-cell lysates is universal with increased pHi.

We next asked what effect decreased pHi had on β-catenin abundance. Despite using several approaches, we were unable to significantly decrease pHi in MDCK cells. Therefore, we used NHE1-deficient PS120 fibroblasts stably expressing either WT NHE1 or a mutant (NHE1-AxxA3) with decreased ion transport activity and a significantly lower pHi (Fig. S3 A; Webb et al., 2016). With lower pHi, the abundance of β-catenin at membrane protrusions was significantly increased (Fig. S3, B and C). Taken together, these data suggest that pHi dynamics regulates β-catenin abundance with increased pHi decreasing abundance of total, membrane-associated, and nuclear β-catenin.

To further determine pHi-dependent effects on β-catenin abundance, we measured protein stability by immunoprecipitating endogenous β-catenin after metabolic pulse–chase labeling in MDCK cells. In controls, β-catenin protein had a half-life of 1.6 ± 0.4 h, but with increased pHi, β-catenin half-life was significantly decreased to 0.5 ± 0.05 h (Fig. 2 F). These data suggest that decreased β-catenin abundance in lysates, at cell–cell junctions, and in the nucleus is due to decreased stability of β-catenin protein at higher pHi.

β-catenin stability is primarily regulated by ubiquitination and proteasome-mediated degradation. The E3 ligase β-TrCP binds the N terminus of β-catenin through interaction with the phosphorylated GSK3β sites and ubiquitinates β-catenin (Fig. 3 A, red box; Hart et al., 1999). The evolutionarily conserved β-TrCP recognition motif contains an invariant histidine (His36 in human β-catenin) between the two serine residues phosphorylated by GSK3β (Fig. 3 B). Histidines (~6.5 pKa) are unique among amino acid residues because they can titrate within the narrow physiological pH range and can function as pH-dependent molecular switches (Schönichen et al., 2013). We previously showed molecular mechanisms for pH-dependent histidine switches in regulating the activity of focal adhesion kinase (Choi et al., 2013), cofilin (Frantz et al., 2008), and the sodium–proton exchanger NHE1 (Webb et al., 2016); however, to our knowledge, the functional significance of histidine in the β-TrCP recognition motif of β-catenin has not been reported.

We first tested whether the histidine in the β-TrCP recognition motif might confer pH-dependent phosphorylation of flanking serine residues by GSK3β. However, in vitro kinase assays

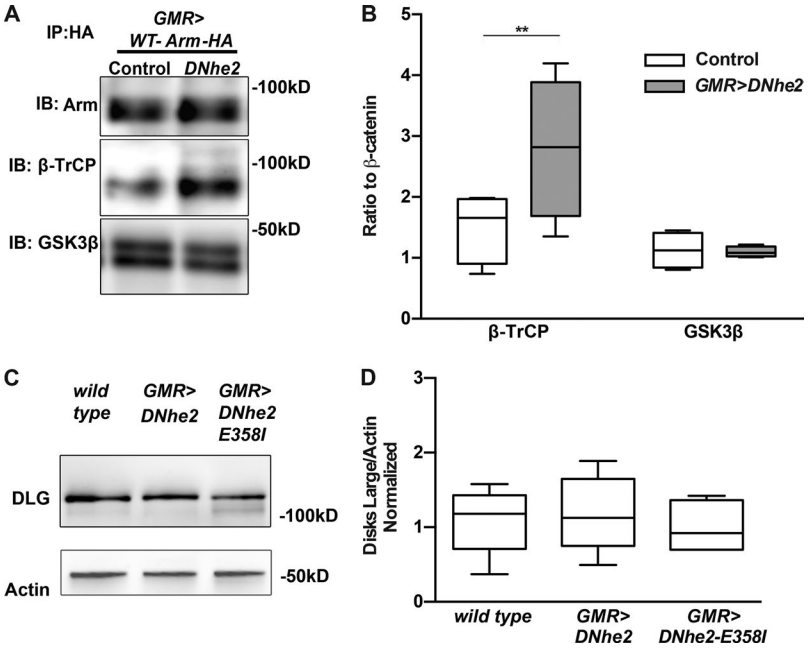

Figure 4. **Higher pHi increases association of β-catenin with the E3 ligase β-TrCP in *Drosophila*. (A)** Representative immunoblots after IP of HA-tagged WT Arm from adult *Drosophila* head lysates without (control) or with *DNhe2* overexpression (*DNhe2*). Immunoblots (IBs) for Arm and GSK3β from immune complexes. **(B)** Quantification of immunoblot replicates performed as described in A. N = 4. **(C)** Representative immunoblots of DLG from adult *Drosophila* head lysates. Lysates were obtained from three *Drosophila* lines: *WT* (*GMR-GAL4*), overexpression of *DNhe2* (*GMR>DNhe2*), and overexpression of a transporter-dead *DNhe2* mutant (*GMR>DNhe2^{E358I}*). **(D)** Quantification of immunoblot replicates performed as described in C. WT and *GMR>DNhe2*, N = 6; *GMR>DNhe2^{E358I}*, N = 4. Tukey boxplots are shown, and significance was determined using an unpaired, two-tailed Student's *t* test with Holm-Sidak's multiple comparisons correction. **, P < 0.01.

performed at buffer pH values of 6.9 and 7.5 using the recombinant N terminus of β-catenin (residues 1–133 fused to GST) revealed pH-insensitive phosphorylation by both the priming kinase CK1 and the processive kinase GSK3β (Fig. 3 C). A published crystal structure of β-TrCP complexed with a double-phosphorylated β-catenin peptide (residues 30–44 with pSer33 and pSer37) shows that β-TrCP WD40 repeats interact electrostatically with β-catenin at both GSK3β phosphorylation sites (Ser33 and Ser37) as well as His36 (Fig. 3 D; Wu et al., 2003). We found a pH-dependent association between endogenous β-catenin and β-TrCP in MDCK cells with increased association at higher pHi. With increased pHi, there was more β-TrCP in β-catenin immune complexes (Fig. 3, E and F) and more β-catenin in β-TrCP immune complexes (Fig. S4, A and B). Additionally, in the presence of the proteasome inhibitor MG132, we observed pH-sensitive changes in ubiquitination of β-catenin, with increased ubiquitination at higher pHi (Fig. 3, E and F). In contrast, we found no pH-dependent changes in β-catenin phosphorylation in MDCK cells, in agreement with our in vitro data (Fig. 3, E and F).

With increased pHi, we found decreased β-catenin in total cell lysates, at cell–cell junctions, and in the nucleus. To examine whether β-TrCP associates with cadherin-bound β-catenin, we used two approaches in MDCK cells. With one approach, we isolated surface proteins using ConA-conjugated beads and found decreased membrane-associated β-catenin at increased pHi (Fig. S4, C and D), which is consistent with our immunolabeling data. However, we were unable to detect membrane-associated β-TrCP, and there was no pHi-dependent difference in E-cadherin abundance. In contrast, with our second approach, we found decreased β-catenin and increased β-TrCP association with endogenous E-cadherin immune complexes at increased pHi (Fig. S4, E and F). These data suggest that β-TrCP can associate with β-catenin–E-cadherin complexes. However, β-TrCP has many cellular targets, and its association specifically with junctional β-catenin and E-cadherin needs further investigation.

We also found increased association of β-TrCP and Arm at higher pHi in *Drosophila* adult head lysates. We generated *Drosophila* lines overexpressing HA-tagged Arm and found that there was increased β-TrCP abundance in HA immune complexes with overexpression of *DNhe2* to increase pHi (Fig. 4, A and B). β-TrCP is one member of a multiprotein destruction complex that also includes APC, Axin, and GSK3β (Wu et al., 2003; Ha et al., 2004; Valenta et al., 2012). Moreover, GSK3β plays a key role in phosphorylating both APC and β-catenin, which is required for efficient β-catenin degradation (Pronobis et al., 2015) and for formation of the destruction complex (Stamos and Weis, 2013). We verified that formation of the destruction complex was independent of pHi, determined by immunoblotting for GSK3β in HA immune complexes (Fig. 4, A and B). β-TrCP has >40 known target proteins (Frescas and Pagano, 2008; Lee and Diehl, 2014), all sharing a conserved destruction recognition motif (DSGXXS), with a subset having a histidine in the second variable position (DSGXHS; Shafique et al., 2016). We therefore tested whether pH-sensitive association of β-catenin and β-TrCP requires a histidine in the destruction site. We monitored the abundance of disks large (DLG), a β-TrCP target lacking a histidine in its destruction recognition motif (DSGPLS), and found that DLG abundance was pH independent in *Drosophila* head lysates (Fig. 4, C and D). These data all suggest specificity for pH-sensitive interaction between β-TrCP and β-catenin.

We next directly tested whether the conserved histidine residue in the DSGIHS destruction motif of β-catenin mediates the pH-sensitive association with β-TrCP. We performed an ELISA binding assay with recombinant β-catenin N terminus (residues 1–133) that we phosphorylated in vitro with CK1 and GSK3β. All proteins were purified to similar purity (Fig. S5). We found pH-dependent binding of recombinant β-TrCP to WT phosphorylated β-catenin, with increased β-TrCP binding at higher pH (Fig. 5, A and E). However, β-TrCP binding to a His36-alanine (Ala) mutant (a nontitratable, neutral substitution) was pH insensitive

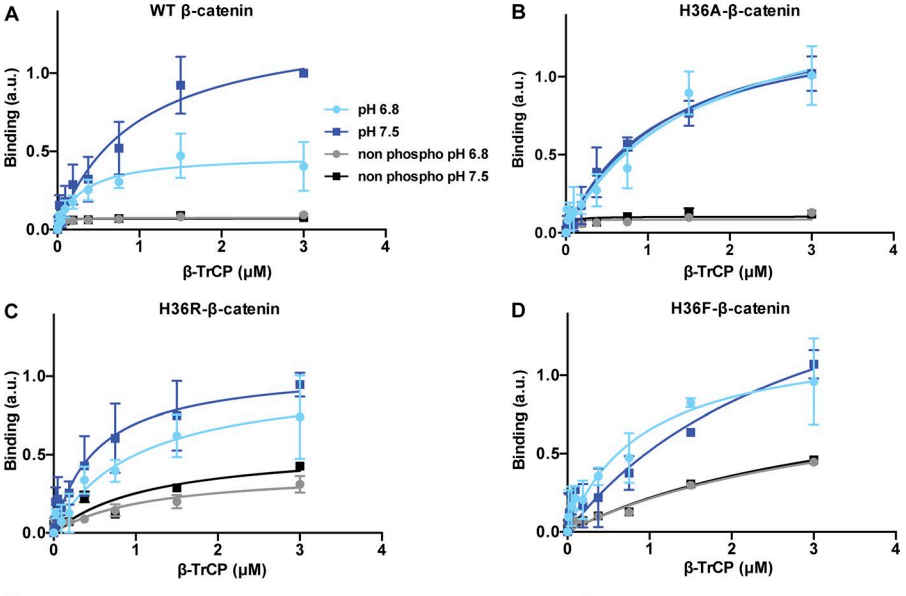

E

	B_{max} (a.u.)		k_d (μM)	
	pH 6.8	pH 7.5	pH 6.8	pH 7.5
WT	0.48 ± 0.04	1.35 ± 0.16 ***	0.29 ± 0.08	0.93 ± 0.27 *
H36A	1.59 ± 0.36 ***	1.39 ± 0.19 ***	1.56 ± 0.72 **	1.12 ± 0.35 *
H36R	1.00 ± 0.15 ***	1.06 ± 0.11 *	0.99 ± 0.35 *	0.51 ± 0.15
H36F	1.26 ± 0.15 ***	2.10 ± 0.83	n.d.	n.d.

F

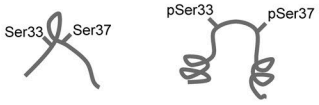

Figure 5. **β-Catenin His36 mediates increased association with β-TrCP at higher pHi in vitro. (A–D)** ELISA assays for in vitro binding of recombinant β-catenin to β-TrCP (see Materials and methods for details) were performed using truncated β-catenin proteins (residues 1–133) expressed as fusions to GST and full-length β-TrCP recombinant protein. The β-catenin fusion proteins were unphosphorylated or phosphorylated in vitro with CK1 and GSK3β. β-TrCP binding at pH 6.8 and 7.5 to WT β-catenin (A), H36A–β-catenin (B), H36R–β-catenin (C), and H36F–β-catenin (D) are shown. N = 3. **(E)** Table of binding constants obtained from β-catenin/β-TrCP binding curves in A–D. Mean ± SD is shown. Significance was determined using an unpaired, two-tailed Student's *t* test with Holm-Sidak's multiple comparisons correction. *, P < 0.05; **, P < 0.01; ***, P < 0.001; n.d., not determined. All compared with WT β-catenin at pH 6.8. **(F)** Model of steric-induced changes in conformation with phosphorylation.

(Fig. 5 B), and binding constants were indistinguishable from WT β-catenin at higher pH (Fig. 5 E). Consistent with β-TrCP binding requiring phosphorylated β-catenin, there was negligible binding of β-TrCP to unphosphorylated WT or H36A–β-catenin at both pH values tested (Fig. 5, A and B). β-TrCP binding to a His36-arganine (Arg) mutant (a nontitratable, positively charged substitution) was pH insensitive; however, there was significant β-TrCP binding to nonphosphorylated H36R–β-catenin (Fig. 5 C). Previous work showed that the N terminus of β-catenin undergoes distinct conformational changes upon phosphorylation (Fig. 5 F; Megy et al., 2005). We predicted that either the increased steric occlusion or charge of the Arg mutation might induce a phosphorylated-like splayed structure even in the nonphosphorylated protein, leading to increased β-TrCP binding to nonphosphorylated H36R–β-catenin. Arg is both bulky and charged, so we also tested a phenylalanine (nontitratable, bulky, and neutral) substitution and observed pH-insensitive β-TrCP binding and significant β-TrCP binding to nonphosphorylated H36F–β-catenin (Fig. 5 D). These data suggest that steric effects are important for specific recognition of phosphorylated β-catenin over nonphosphorylated β-catenin (Fig. 5 F) and that both established steric constraints conferred by phosphorylation and charge effects at His36 coincide to regulate β-TrCP recognition of β-catenin.

Somatic mutation of the conserved His36 to Arg has been identified in several cancers in the Catalog of Somatic Mutations in Cancer database (Forbes et al., 2015); however, to our knowledge, the functional consequences of this mutation have not been reported. We generated transgenic *Drosophila* lines with inducible expression of WT Arm (*UAS-arm*), with the analogous His42-Arg mutation (*UAS-arm^{H42R}*), and an Ala substitution His42-Ala (*UAS-arm^{H42A}*). Transgenes were expressed using *eyeless-GAL4* (*eyGAL4*) at moderate levels in retinal tissues from the time of specification in embryos through adulthood. Expression of WT *arm* showed no patterning defects in the eye (Fig. 6, A and B), and the *arm^{H42A}* mutation showed ∼55% WT eyes, ∼37% eyes with mildly rough patches, and ∼8% eyes with slight overgrowth (Fig. 6, A and B). In contrast, all eyes expressing *arm^{H42R}* showed profound defects in retinal patterning, with specific defects including reduced rough eyes (∼59%), overgrown bulging eyes (∼19%), reduced split eyes (∼8%), missing eyes (∼5%), and strikingly large protruding tumors (∼8%; Fig. 6, A and B). Histological sections through these tumors revealed mostly well-differentiated photoreceptor neurons, with a few ommatidia missing a full complement of eight photoreceptor neurons (Fig. 6 C, black circles). Similar phenotypes were reported with *eyGAL4*-expressed transgenes that activate Wnt signaling in the eye, where expression of RNAi targeting *slimb* (*Drosophila* β-TrCP homologue) or *shaggy* (*Drosophila* GSK-3β homologue) induced overgrowth or protruding tumors, respectively, while overexpression of *dishevveled* showed the reduced, split-eye phenotype (Reim et al., 2014). In addition, histological sections of tumors induced by *arm^{H42R}* revealed significant planar cell polarity errors, including inversions on the dorsal–ventral and anterior–posterior axes (Fig. 6 C); the penetrance of these errors was so high that it was impossible to discern the axes of the eye from these sections. We compared the penetrance of these phenotypes to the classic gain-of-function, stabilized mutant-variant *arm^{S10}* (Pai et al., 1997), where a portion of the N terminus containing the phosphorylated and ubiquitinated residues is deleted. With expression of *arm^{S10}*,

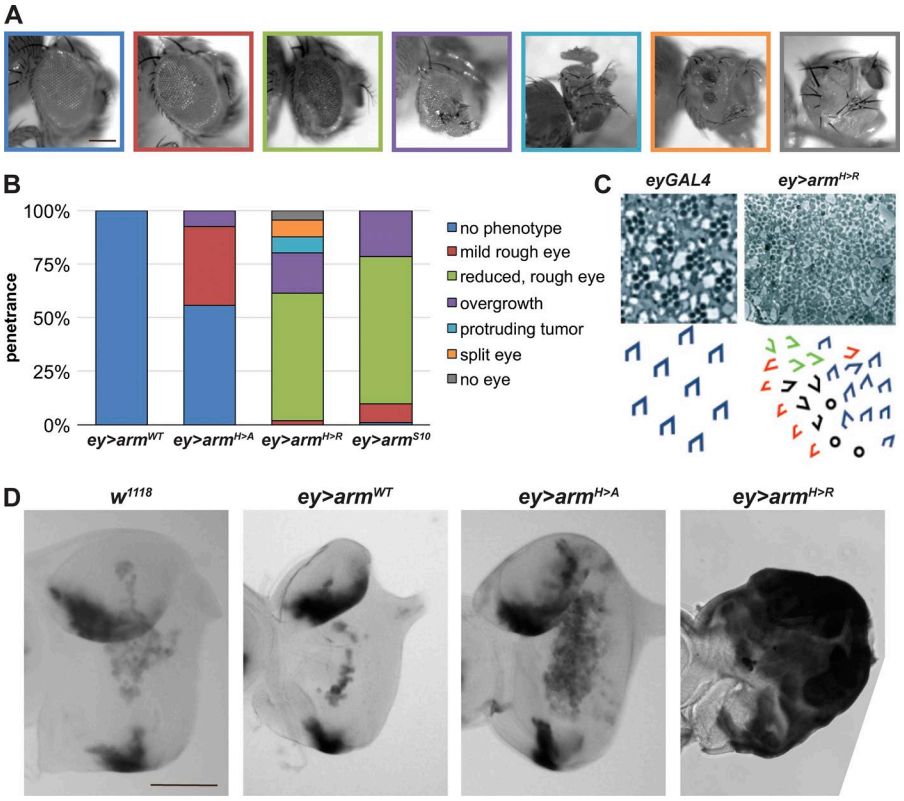

Figure 6. **Mutation of pH-sensing histidine to Arg in β-catenin induces ectopic tumors in *Drosophila* eyes. (A)** Photomicrographs show external eye morphologies in flies expressing the indicated Arm mutants using *eyGAL4*. Images are outlined with colors that correspond with the graph in B as follows (left to right): blue (no phenotype), red (mild rough eye), green (reduced rough eye), purple (overgrowth), aqua (protruding tumor), orange (split eye), and gray (no eye tissue). **(B)** Penetrance of phenotypes shown in A for *ey>Arm*-expressing flies. **(C)** Histological sections through protruding tumors seen with $Arm^{H>R}$ show defects in cell fate specification and ommatidial orientation with different chiral forms of ommatidia shown in blue, red, green, and black, and ommatidia with missing photoreceptors are shown as black circles. **(D)** Representative images of third larval instar eye imaginal discs expressing the notum-lacZ Wnt pathway reporter with *UAS-arm* and *eyGAL4* transgenes. Discs were stained with X-gal to indicate Wnt pathway activity. Bars, 100 µm. w^{1118}, N = 22; $UAS\text{-}arm^{WT}$, N = 10; $UAS\text{-}arm^{H>A}$, N = 13; $UAS\text{-}arm^{H>R}$, N = 5.

~9% of eyes were mildly rough, ~67% were reduced and rough, and ~21% showed overgrown, bulging eyes. The appearance of unique phenotypes in arm^{H42R} that are not seen with arm^{S10} suggests that this mutation may act as a neomorph, conferring novel protein functions.

To determine whether these mutations affect canonical Wnt signaling, we generated flies expressing our *UAS-arm* transgenes under control of *eyGAL4* with the established transcriptional reporter notum-lacZ (Liu et al., 2008). Reporter expression in third larval instar eye imaginal discs was examined using X-gal staining. In control crosses with the WT strain w^{1118}, notum-lacZ expression is restricted to the dorsal and ventral poles of the eye imaginal disc in two distinct patches (Fig. 6 D). Flies with $ey{>}arm^{WT}$ or $ey{>}arm^{H42A}$ express these transgenes throughout the eye disc but showed a similar pattern to control, suggesting that endogenous degradation mechanisms are sufficient to prevent ectopic Wnt signaling for these transgenes (Fig. 6 D). However, flies expressing $ey{>}arm^{H42R}$ showed elevated Wnt activity throughout the eye disc in all samples examined (Fig. 6 D). These data indicate that when the arm^{H42R} mutant is expressed at physiologically relevant levels, it is both resistant to endogenous degradation mechanisms and sufficient to induce aberrant Wnt signaling.

Discussion

Our work identifies pHi dynamics as a previously unrecognized regulator of β-catenin stability. We show that β-catenin is a pH sensor, and at higher pHi, it has decreased abundance in whole lysates, at adherens junctions, and in the nucleus. We suggest a neutral (deprotonated) histidine in the destruction motif DSG XHS functions in coincidence with obligatory phosphorylation of N-terminal residues (Aberle et al., 1997; Daugherty and Gottardi, 2007) to enable β-catenin binding to the E3 ligase β-TrCP. We previously reported that cofilin, an actin-binding protein and pH sensor, also requires a neutral histidine (His133 human cofilin) in coincidence with an obligatory N-terminal phosphorylation (pSer3) for increased activity (Frantz et al., 2008). The DSGXHS degradation motif with an invariant histidine in β-catenin also occurs in a number of other proteins, and an important future direction is to determine whether the invariant histidine confers pHi-dependent changes in stability in those proteins as well. Our work reveals an unexplored effect of pHi dynamics on proteasome-mediated protein stability: if this pHi-dependent regulation is common to a subset of β-TrCP targets, it may enable coordinated cellular responses to increased pHi.

A number of normal cell behaviors regulated by pHi dynamics including migration (Denker and Barber, 2002; Choi et al., 2010; Parks and Pouyssegur, 2015), differentiation (Ulmschneider et al., 2016), and tumorigenesis (Reshkin et al., 2014; White et al., 2017b) are also regulated by Wnt signaling (Krausova and Korinek, 2014; Sedgwick and D'Souza-Schorey, 2016). For example, in follicle stem cells of the *Drosophila* germarium, Wnt signaling is high and decreases in differentiated daughter follicle cells (Sahai-Hernandez et al., 2012; Dai et al., 2017; Waghmare and Page-McCaw, 2018), and we recently showed that pHi is lower in follicle stem cells, with an obligatory increase for differentiation of follicle cells (Ulmschneider et al., 2016). Future work testing these collective findings will be important for understanding how pHi dynamics cross-talks with both Wnt signaling and other signaling pathways in normal and pathological cellular processes.

The regulation of β-catenin stability by pHi dynamics likely has previously unrecognized roles in cancer. Most cancers have a constitutively increased pHi >7.4 (White et al., 2017b), and increased pHi is sufficient to induce dysplasia in the absence of activated oncogenes (Grillo-Hill et al., 2015). Relevant to cancer, our findings using the *Drosophila* transcriptional reporter notum-LacZ suggest that an H36R–β-catenin somatic mutation in human cancers (Forbes et al., 2017) can bypass pH-sensitive β-TrCP recognition and increase Wnt pathway activity. Past work by Simons et al. (2009) showed that increased pHi induced by overexpression of a *Drosophila* Na–H exchanger promotes noncanonical Wnt signaling; however, no discernable effects on canonical Wnt signaling were found. Our work adds to the growing body of data suggesting pHi as a regulator of diverse cellular signaling processes and supports future studies determining whether pH-dependent cancer cell behaviors are in part mediated by pH-dependent changes in β-catenin stability such as loss of cell–cell junctions for tumor cell metastasis.

Materials and methods

Drosophila lines and genetics

Flies were grown on standard *Drosophila* media and cultured at 25°C. The following lines were used: *GMRGAL4* (from R. Cagan, Mount Sinai School of Medicine, New York, NY); yw; Notum-lacZ; (from K. Cadigan, University of Michigan, Ann Arbor, MI); w; *UAS-DNhe2* (described by Grillo-Hill et al., 2015); y[1] w[1118]; P{w[+mC]=UAS-arm.S2}A1 (*UAS-arm*; 4783; Bloomington Drosophila Stock Center [BDSC]); y[1] v[1]; P{y[+t7.7] v[+t1.8]=TRiP.JF01251}attP2/TM3, Ser[1] (*UAS-arm.RNAi4*; 31304; BDSC); y[1] v[1]; P{y[+t7.7] v[+t1.8]=TRiP.JF01252}attP2 (*UAS-arm.RNAi5*; 31305; BDSC); w[1118]; P{w[+mC]=UASp-shg.GFP}5B (*UAS-shg::GFP*; 58445; BDSC); w[1118]; P{y[+t7.7] w[+mC]=UASp-shg.S}attP2 (*UAS-shg*; 65589; BDSC); P{w[+mC]=UAS-arm.S10}C, y[1] w[1118] (*UAS-Arm.S10*4782; BDSC); y[1] w[1118]; P{w[+mC]=ey3.5-GAL4.Exel}3, (*eyGAL4*; 8219; BDSC); and pnut[XP]/T(2;3)SM6a-TM6B, Tb[1] (*SM6a-TM6B*; 5687; BDSC).

The *arm* cDNA was obtained from a public stock center (cDNA clone LD23131; Drosophila Genomics Resource Center) and cloned into pUASt-HA to generate an HA tag at the C terminus of the protein to distinguish endogenous from transgenic protein. Transgenic flies were generated (BestGene, Inc.) and phenotypically tested, and protein expression levels were empirically determined. For these studies, we selected lines with high and low protein expression levels and saw identical results for both.

Scanning EM

Adult heads were removed, bisected sagittally, and fixed overnight in 2% glutaraldehyde + 4% paraformaldehyde in 0.1 M sodium phosphate buffer, pH 7.4. Samples were processed in a critical point dryer, mounted on carbon tape (16,084-6; Ted Pella) or with colloidal silver (16,034; Ted Pella) on an scanning EM stub (16,221; Ted Pella) and splutter coated with gold-palladium (22-2; Ted Pella). Images were collected on a JEOL Neoscope scanning electron microscope and cropped in Photoshop (Adobe).

Antibodies

For *Drosophila* immunolabeling, the following antibodies were obtained from the Developmental Studies Hybridoma Bank (DSHB; created by the National Institute of Child Health and Human Development of the National Institutes of Health and maintained at The University of Iowa): Arm (N2 7A1; 1:10; deposited to the DSHB by E. Wieschaus, Princeton University, Princeton, NJ), Shg (DCAD2; 1:10; deposited to the DSHB by T. Uemura, Kyoto University, Kyoto, Japan), and N_cadherin (DN-Ex 8; 1:10; deposited to the DSHB by T. Uemura). For MDCK immunolabeling, the following antibodies were used: mouse anti–β-catenin (1:400; 610154; BD) and rat anti–E-cadherin (1:400; 13-1900; Invitrogen).

Tissue histology and quantitative image analysis

Drosophila pupal retinal tissues were dissected in PBS, fixed in fresh 4% paraformaldehyde for 30 min, washed in PBS + 0.1% Triton X-100, and immunostained with primary antibodies overnight at 4°C and secondary antibodies for 60 min at RT in the dark. Mammalian cells were grown as described below, fixed on ice for 20 min in fresh 4% paraformaldehyde, washed in PBS, blocked in PBS + 5% goat serum + 0.3% Triton X-100 for 15 min at RT, and washed in PBS. Fixed cells were immunostained with primary antibodies overnight at 4°C and secondary antibodies for 60 min at RT in the dark. Samples were mounted in Prolong Gold (P36930; Thermo Fisher Scientific). Confocal images were collected on an inverted spinning-disk confocal microscope (Stehbens et al., 2012). NIS Elements software (Nikon) was used to subtract background and measure fluorescence intensity in individual channels. For display purposes, single-channel images were exported, and the lookup table "Fire" was applied in FIJI (ImageJ; National Institutes of Health). For intensity measurements, fluorescence intensity measurements were collected from a single region of interest per cell–cell junction in the Z section with highest intensity for that junction. Statistical analyses were performed using Prism (GraphPad Software). First, data were subjected to the D'Agostino and Pearson omnibus normality test, and all datasets showed a nonnormal distribution. Outliers were removed using the robust regression and outlier removal (ROUT) method. Where indicated, data were next normalized within each biological replicate to the mean intensity for all control junctions. Data were then subjected to the Mann–Whitney nonparametric test to determine significance.

Adult eye tissue dissection, fixation, and resin embedding were performed as described previously (Wolff, 2000). Tissue was cut into 0.5-µm sections on a microtome and contrast stained with toluidine blue. Phase-contrast images were collected on a Zeiss Axiophot microscope using a 63× oil objective and a Hamamatsu ORCA-ER digital camera. Images were cropped, pseudocolored, and brightness/contrast adjusted in Photoshop.

For Wnt reporter assays, flies expressing *UAS-arm* transgenes under the *eyeless-GAL4* driver were generated and balanced over the SM6a-TM6B compound balancer. Genotypes were verified by PCR, where both wings were removed from individual male flies and used as the source for the genomic DNA. Males carrying both the *GAL4* and *UAS* transgenes balanced over SM6a-TM6B were mated to *notum-lacZ* virgin females. Resulting offspring were grown to wandering third instar larvae and then dissected, and

eye imaginal discs were fixed in 1% glutaraldehyde for 15 min at RT and permeabilized in 0.3% Triton X-100 in PBS. X-gal staining was performed as described previously (Cold Spring Harbor Protocols, 2010). Tissues were mounted in glycerol and imaged as described above.

Protein lysate preparation from whole *Drosophila* heads

Drosophila heads were dissected into cold radioimmunoprecipitation assay buffer (Peifer, 1993; 300 mM NaCl, 50 mM Tris-HCl, pH 8.5, 1% NP-40, 0.5% sodium deoxycholate, 0.1% SDS, 2 mM $CaCl_2$, 1% Triton X-100, 1% NP-40 in PBS plus 10 mM DTT, 1 mg/ml PMSF, 10 mM Na_3VO_4, 10 mM NaF, and EDTA-free complete protease inhibitors [Roche]) at 2–3 µl per head. Heads were homogenized with a pestle, incubated for 60 min on ice, and then sonicated on ice for six rounds of 30-s sonication with 90 s rest on ice. Lysates were centrifuged for 15 min at 4°C at 15,000 *g* in an Eppendorf centrifuge. For each condition, 10 heads were loaded onto 10% SDS-PAGE gels and run at 120 V for 1.2 h. Proteins were transferred (25 mM Tris, 192 mM glycine, 20% methanol, and 0.01% SDS) onto polyvinylidene difluoride (PVDF) membranes at 100 V for 1.5 h. Membranes were blocked for 1 h in 5% nonfat milk in TBS-T (TBS with 0.1% Tween-20) with shaking at RT. Primary antibodies were diluted in 5% nonfat milk in TBS-T and incubated overnight with shaking at 4°C. Arm (1:500; N2 7A1), Shg (1:1,000; DCAD2), N_cadherin (1:1,000; DN-Ex 8), DLG (1:1,000; 4F3), and actin (1:5,000; C4; EMD Millipore). Membranes were washed in TBS-T (3 × 5 min) with shaking. Appropriate secondary antibodies were diluted 1:10,000 in 5% nonfat milk in TBS-T and incubated for 1 h with shaking at RT (Bio-Rad anti–mouse-HRP [170-6516] and anti–rabbit-HRP [172-1019]). Membranes were washed in TBS-T (3 × 5 min) with shaking, developed (SuperSignal West Femto; Pierce), and visualized (Alpha Innotech FluorChem Q).

Cell culture, pHi control, and measurement

MDCK (ATCC): Eagle's minimum essential medium + 10% FBS. NMuMG cells: DMEM supplemented with 10% FBS and 10 µg/ml insulin. PS120 cells: DMEM supplemented with 5% FBS. MDCK, NMuMG, or PS120 cells were plated (6.0×10^4 cells per six-well plate for MDCK, 4.0×10^4 for NMuMG, or 5.0×10^4 for PS120). For acute pHi control, cells were incubated in complete medium supplemented with 5 mM ammonium chloride for 24 h. For chronic pHi control, MDCK cells were placed in an incubator with atmospheric conditions of 15% CO_2 for two passages (10 d) and increased HCO_3 in the media to 30 mM. Where indicated, the proteasome inhibitor MG132 (S2619; SelleckChem) was added to a final concentration of 10 µM for the final 6 h of the experiment. Steady-state pHi was measured as previously described (Choi et al., 2013). For all conditions, triplicate wells were plated (2×10^4 per well; 24-well plate). Technical replicates were averaged within each biological replicate.

Mammalian cell lysate preparation

Cells were washed twice with ice-cold PBS and incubated with 100 ml ice-cold lysis buffer (50 mM Tris, 150 mM NaCl, 1 mM NaF, 1% Triton X-100, and protease inhibitor cocktail [Roche], pH 7.5) for 10 min on ice. Cells were scraped, and clarified lysate (10,000 rpm; 10 min) was used immediately for immunoprecipitation (IP), immunoblotting, or flash freezing and storage at −80°C.

Immunoblotting of mammalian cell lysates

Proteins were transferred to 0.45-µm PVDF membranes (100 V for 1 h on ice; Immobilon) in modified transfer buffer (Tris-Gly, 20% MeOH, and 0.01% SDS) to maximize transfer of ubiquitinated β-catenin. Membranes were blocked in 5% BSA in TBS-T (0.1% Tween-20 in TBS) for 1 h at RT and then divided for blotting. Primary antibodies: total β-catenin (1:1,000; 610154; BD), pSer (33/37) pThr41 β-catenin (1:1,000; 9561; Cell Signaling Technology), pSer45 β-catenin (1:1,000; 9564; Cell Signaling Technology), and β-TrCP (1:1,000; D13F10; 4349; Cell Signaling Technology), ubiquitin (1:2,000; 3933; Cell Signaling Technology), and E-cadherin (1:2,000; 610181; BD). Primary antibodies were used at indicated dilutions in 5% BSA/TBS-T and incubated overnight with shaking at 4°C. Membranes were washed with shaking (3 × 5 min; TBS-T). Secondary HRP-conjugated antibodies against mouse or rabbit (1706515 and 1721019; Bio-Rad; 1:10,000 in 5% BSA/TBS-T) were incubated for 1 h (RT with shaking). Membranes were washed with shaking (3 × 5 min; TBS-T), developed (SuperSignal West Femto; Pierce), and visualized (Alpha Innotech FluorChem Q).

IP assays in cells

Cell lysates were prepared as described above. 250 µl lysate was combined with 1–2 µl anti–β-catenin antibody (AB19022 [discontinued; EMD Millipore] or 9562 [Cell Signaling Technology] for β-TrCP coimmunoprecipitations; 610154 [BD] for ^{35}S metabolic pulse–chase assays), anti–β-TrCP antibody (D13F10; 4394; Cell Signaling Technology), or anti–E-cadherin antibody (610181; BD). Antibody and lysate were incubated on a nutator overnight at 4°C. After overnight incubation, 30–40 µl protein G-Mag Sepharose slurry (28-9440-08; GE Healthcare) was added to each tube and incubated on a nutator for 3 h at 4°C. Protein G-Mag Sepharose beads were separated by magnet, and supernatant was removed. Beads were washed 3× with 800 µl wash buffer (TBS + 0.1% Triton X-100 and protease inhibitor cocktail). Protein was eluted from washed beads by incubating at 50°C for 5 min with 40 µl 2× loading buffer (Bio-Rad) without DTT. Beads were separated by magnet, elution was removed, and DTT was then added to a final concentration of 100 mM. For ConA separations, 30 µl ConA-conjugated agarose (786-216; G-biosciences) was added to lysates and incubated overnight on a nutator at 4°C. Washes were all performed as described above, spinning agarose between washes at 500 rpm for 2 min at 4°C. For all conditions, 5–10 µl of the elutions was run on 10% SDS-PAGE gels. For representative blots in Fig. 3, equal amounts of β-catenin protein loading were achieved by adding 50% more elution in the high-pH conditions. Immunoblotting was performed as described above.

^{35}S metabolic labeling pulse–chase assays

MDCK cells were plated at 8.0×10^4 cells per 35-mM dish with eight total dishes plated. 24 h after plating, half of the dishes were treated with 5 mM ammonium chloride. 48 h after plating, cells were starved of methionine by washing and incubating for 30 min in methionine-free media (Eagle's minimum essential me-

dium without methionine and cysteine [1641454; MB-bio] supplemented with 10 mM cysteine, 2 mM glutamine, and 10% FBS). Note that for this and all future steps, 5 mM ammonium chloride was supplemented to media and washes for the high-pHi conditions. After methionine depletion, cells were incubated with 0.5 ml methionine-free media supplemented with 0.5–0.625 mCi/ml ^{35}S-methionine (NEG009A; PerkinElmer) for 30 min. Cells were washed 3× in complete media, and time-0 lysates were prepared as described above for control and ammonium chloride conditions. All other plates were returned to the incubator, and matched plates were lysed 1 h, 2 h, and 4 h later. For two of the four replicates, the experiment was performed as described above except using double-labeled ^{35}S-methionine/^{35}S-cysteine (NEG772; PerkinElmer) supplemented at 0.5–0.875 mCi/ml. For these conditions, cells were starved of methionine and cysteine by washing and incubating for 30 min in methionine/cysteine-free media (Eagle's minimum essential medium without methionine and cysteine [1641454; MB-bio] supplemented with 2 mM glutamine and 10% FBS).

250 µl of each labeled lysate was combined with 1 µl anti–β-catenin antibody (610154; BD). Antibody and lysate were incubated on a nutator overnight at 4°C. After overnight incubation, 30–40 µl protein G-Mag Sepharose slurry (28-9440-08; GE Healthcare) was added to each tube and incubated on a nutator for 3 h at 4°C. Protein G-Mag Sepharose beads were washed as described above, and protein was eluted from washed beads by boiling at 95°C in 25 µl 2× Laemmli buffer with DTT. The entire elution was run on a 10% SDS-PAGE gel, which was then stained for 1 h in Instant Blue (1SB1L; Expedeon). After destaining, an image was acquired, and then gels were fixed (10% acetic acid and 40% methanol in water) for 5 min, rehydrated in 2% glycerol in water for 5 min, and then incubated in FluorHance (Research Products International) for 30 min before drying (model 853; Bio-Rad). Autoradiograph film (E3018; Denville Hyblot CL) was exposed for 1–2 wk at −80°C. Densitometry results from the autoradiograph were normalized to amount of protein detected in IP by InstantBlue staining.

IP assays from *Drosophila* head lysates

Drosophila heads were harvested and prepared as described above. For each IP sample, clarified lysate from 100 heads were combined with 2 µl anti-HA antibody (HA.11; 16B12; Covance), and IPs were performed as described above for mammalian cells. Elution volume for each IP sample was 30 µl, and 15 µl was run on 10% SDS-PAGE gels. Immunoblotting was performed as described above using anti-Arm (1:500; N2 7A1; DSHB), anti–β-TrCP (1:200; D13F10; 4394; Cell Signaling Technology), and anti-GSK3β (1:2,000; 05-412; EMD Millipore).

In vitro expression, purification, and phosphorylation of β-catenin (1–133)

Original WT β-catenin (residues 1–133 fused to GST) was generously provided by B. Weis (Stanford University, Stanford, CA). Point mutations (H36A, H36R, and H36F) were introduced using standard QuikChange protocol (Stratagene). Resulting constructs were transformed into and expressed in BL21-DE3 *Escherichia coli*. Cells were grown in Luria broth + 50 µg/ml ampicillin (37°C; with shaking) until OD_{600} = 0.6 and induced (0.5 mM IPTG for 5 h at RT with shaking). Cells were pelleted (6,000 *g* for 10 min at 4°C), resuspended in lysis buffer (25 mM Tris, pH 7.5, 150 mM NaCl, 1 mM EDTA, and protease inhibitor cocktail), and lysed by sonicating 6 × 30 s (cooling lysate for 2 min between sonication pulses). Clarified supernatant (14,000 *g* for 10 min at 4°C) was loaded onto to a preequilibrated glutathione-agarose column (Thermo Fisher Scientific) and washed with 20 column volumes lysis buffer, and then the protein was eluted in binding buffer with 15 mM reduced glutathione, pH 8.0. Proteins were dialyzed into storage buffer (20 mM Tris, 50 mM NaCl, 1 mM DTT, and 5% glycerol, pH 7.5) and concentrated. Aliquots were flash frozen in liquid nitrogen and stored at −80°C.

For kinase reactions, 15 µg purified β-catenin–GST was incubated with 0.4 µg recombinant CK1 (SRP5013; Sigma-Aldrich) either with or without 0.2 µg recombinant GSK3β (G4296; Sigma-Aldrich). Reactions were performed in 50 mM Hepes buffer containing 5 mM ATP, 10 mM $MgCl_2$, and 5 mM DTT, pH 6.9 or 7.5, for 1 h at 30°C. Reactions were quenched with EDTA (C_f = 100 mM). Each reaction was boiled in 1× Laemmli buffer for 5 min and then divided in half and run in duplicate on 12% SDS-PAGE gel at 100 V for 90 min. Western blotting for phospho–β-catenin was performed as described above.

ELISA β-catenin (1–133) and β-TrCP binding assay

30 µg purified protein was phosphorylated as described above at buffer pH 7.5 for 4 h to ensure complete phosphorylation. Phosphorylated or nonphosphorylated β-catenin was immobilized on high-binding ELISA plates at 4 µg/ml in PBS overnight with shaking at 4°C. Plates with immobilized protein were washed 2× with PBS and then blocked with 5% milk in PBS overnight with shaking at 4°C. Blocked plates were washed 2× with PBS, and then WT β-TrCP was incubated at concentrations from 0–1 µM in binding buffer (20 mM Hepes, 150 mM NaCl, and 1% goat serum) at pH 6.8 or 7.5 for 90 min at RT with shaking. Plates were washed with wash buffer (binding buffer + 0.05% Tween-20) 3 × 5 min and then incubated for 2 h with anti–β-TrCP (D13F10; 4394; Cell Signaling Technology) diluted 1:1,000 in binding buffer. Plates were washed with wash buffer for 3 × 5 min and then incubated for 90 min with anti–rabbit-HRP (1721019; Bio-Rad) at 1:5,000 dilution. Plates were washed with wash buffer for 3 × 5 min, 100 µl 3,3′,5,5′-tetramethylbenzidine (T8665; Sigma-Aldrich) was added to each well for 15 min, and the optical density was read at 370 nM on a SpectraMax M5 plate reader.

Statistical analysis

Statistical analyses used to compare datasets are described in the figure legends. N indicates number of biological replicates, while n indicates number of technical replicates (or individual measures where applicable). Where appropriate and where indicated, medians were displayed instead of means. Statistical tests used for normality testing (where applicable) are described in Materials and methods.

Online supplemental material

Fig. S1 shows that overexpression of *DNhe2* has no effect on total cadherins and mixed effects on cadherin localization at cell–cell

contacts. Fig. S2 shows that higher pHi decreases β-catenin total and junctional abundance in NMuMG epithelial cells and in MDCKs (15% CO_2); while total E-cadherin levels are unchanged with altered pHi, junctional levels in MDCKs are altered. Fig. S3 shows that lower pHi increases β-catenin abundance at membrane protrusions in fibroblasts. Fig. S4 shows that higher pHi increases association of β-catenin with the E3 ligase β-TrCP and increases the amount of β-TrCp associating with cadherin-associated β-catenin. Fig. S5 shows a Coomassie stain of purified β-catenin–(1–133)-GST proteins.

Acknowledgments

We thank Changhoon Choi for assistance on the early stages of the project, Marian Baquilar for assistance with screening and genetic interactions, and Luke Miller, Bill Weis, James Nelson, Torsten Wittmann, and members of the Wittmann and Barber laboratories for helpful discussions. *Drosophila* fly lines were obtained from the Drosophila Genomics Resource Center, supported by National Institutes of Health grant 2P40OD010949, and plasmids for in vitro β-catenin–(1–133)-GST were provided by B. Weis.

This work was supported by National Institutes of Health grants CA197855 and GM116384 to D.L. Barber, National Institutes of Health F32 grant CA177085 to K.A. White, and startup funding from the San Jose State University Department of Biological Sciences and College of Sciences to B.K. Grillo-Hill.

The authors declare no competing financial interests.

Author contributions: K.A. White and B.K. Grillo-Hill contributed equally to this work. B.K. Grillo-Hill prepared all *Drosophila* reagents and performed screening of genetic interactions, scanning EM, histology, immunolabeling, and image analysis, and they also prepared fly head lysates. K.A. White performed biochemical and cell biology analyses, metabolic pulse–chase labeling, pH measurements, and image analysis. M. Esquivel, J. Peralta, V.N. Bui, and I. Chire screened for genetic interactions. J. Peralta, V.N. Bui, and I. Chire assisted with the Wnt reporter assays in flies. D.L. Barber performed pH measurements, immunolabeling, metabolic pulse–chase labeling, and image analysis. D.L. Barber, K.A. White, and B.K. Grillo-Hill conceived experiments, performed data analysis, and wrote the manuscript. D.L. Barber should be contacted for any cell biological or biochemical questions/reagents. B.K. Grillo-Hill should be contacted for any *Drosophila* questions/reagents.

Submitted: 7 December 2017
Revised: 16 July 2018
Accepted: 31 August 2018

References

Aberle, H., A. Bauer, J. Stappert, A. Kispert, and R. Kemler. 1997. beta-catenin is a target for the ubiquitin-proteasome pathway. *EMBO J.* 16:3797–3804. https://doi.org/10.1093/emboj/16.13.3797

Baumgartner, M., H. Patel, and D.L. Barber. 2004. Na(+)/H(+) exchanger NHE1 as plasma membrane scaffold in the assembly of signaling complexes. *Am. J. Physiol. Cell Physiol.* 287:C844–C850. https://doi.org/10.1152/ajpcell.00094.2004

Chairoungdua, A., D.L. Smith, P. Pochard, M. Hull, and M.J. Caplan. 2010. Exosome release of β-catenin: a novel mechanism that antagonizes Wnt signaling. *J. Cell Biol.* 190:1079–1091. https://doi.org/10.1083/jcb.201002049

Choi, C.H., H. Patel, and D.L. Barber. 2010. Expression of actin-interacting protein 1 suppresses impaired chemotaxis of Dictyostelium cells lacking the Na+-H+ exchanger NHE1. *Mol. Biol. Cell.* 21:3162–3170. https://doi.org/10.1091/mbc.e09-12-1058

Choi, C.H., B.A. Webb, M.S. Chimenti, M.P. Jacobson, and D.L. Barber. 2013. pH sensing by FAK-His58 regulates focal adhesion remodeling. *J. Cell Biol.* 202:849–859. https://doi.org/10.1083/jcb.201302131

Cold Spring Harbor Protocols. 2010. X-gal staining solution for Drosophila eyes. *Cold Spring Harb. Protoc.* https://doi.org/10.1101/pdb.rec12207

Dai, W., A. Peterson, T. Kenney, H. Burrous, and D.J. Montell. 2017. Quantitative microscopy of the Drosophila ovary shows multiple niche signals specify progenitor cell fate. *Nat. Commun.* 8:1244. https://doi.org/10.1038/s41467-017-01322-9

Daugherty, R.L., and C.J. Gottardi. 2007. Phospho-regulation of Beta-catenin adhesion and signaling functions. *Physiology (Bethesda).* 22:303–309.

Denker, S.P., and D.L. Barber. 2002. Cell migration requires both ion translocation and cytoskeletal anchoring by the Na-H exchanger NHE1. *J. Cell Biol.* 159:1087–1096. https://doi.org/10.1083/jcb.200208050

Denker, S.P., D.C. Huang, J. Orlowski, H. Furthmayr, and D.L. Barber. 2000. Direct binding of the Na--H exchanger NHE1 to ERM proteins regulates the cortical cytoskeleton and cell shape independently of H(+) translocation. *Mol. Cell.* 6:1425–1436. https://doi.org/10.1016/S1097-2765(00)00139-8

Endo, K., T. Ueda, J. Ueyama, T. Ohta, and T. Terada. 2000. Immunoreactive E-cadherin, alpha-catenin, beta-catenin, and gamma-catenin proteins in hepatocellular carcinoma: relationships with tumor grade, clinicopathologic parameters, and patients' survival. *Hum. Pathol.* 31:558–565. https://doi.org/10.1053/hp.2000.6683

Forbes, S.A., D. Beare, P. Gunasekaran, K. Leung, N. Bindal, H. Boutselakis, M. Ding, S. Bamford, C. Cole, S. Ward, et al. 2015. COSMIC: exploring the world's knowledge of somatic mutations in human cancer. *Nucleic Acids Res.* 43(D1):D805–D811. https://doi.org/10.1093/nar/gku1075

Forbes, S.A., D. Beare, H. Boutselakis, S. Bamford, N. Bindal, J. Tate, C.G. Cole, S. Ward, E. Dawson, L. Ponting, et al. 2017. COSMIC: somatic cancer genetics at high-resolution. *Nucleic Acids Res.* 45(D1):D777–D783. https://doi.org/10.1093/nar/gkw1121

Frantz, C., G. Barreiro, L. Dominguez, X. Chen, R. Eddy, J. Condeelis, M.J. Kelly, M.P. Jacobson, and D.L. Barber. 2008. Cofilin is a pH sensor for actin free barbed end formation: role of phosphoinositide binding. *J. Cell Biol.* 183:865–879. https://doi.org/10.1083/jcb.200804161

Frescas, D., and M. Pagano. 2008. Deregulated proteolysis by the F-box proteins SKP2 and beta-TrCP: tipping the scales of cancer. *Nat. Rev. Cancer.* 8:438–449. https://doi.org/10.1038/nrc2396

Grillo-Hill, B.K., C. Choi, M. Jimenez-Vidal, and D.L. Barber. 2015. Increased H^+ efflux is sufficient to induce dysplasia and necessary for viability with oncogene expression. *eLife.* 4:e03270. https://doi.org/10.7554/eLife.03270

Ha, N.C., T. Tonozuka, J.L. Stamos, H.J. Choi, and W.I. Weis. 2004. Mechanism of phosphorylation-dependent binding of APC to beta-catenin and its role in beta-catenin degradation. *Mol. Cell.* 15:511–521. https://doi.org/10.1016/j.molcel.2004.08.010

Hart, M., J.P. Concordet, I. Lassot, I. Albert, R. del los Santos, H. Durand, C. Perret, B. Rubinfeld, F. Margottin, R. Benarous, and P. Polakis. 1999. The F-box protein beta-TrCP associates with phosphorylated beta-catenin and regulates its activity in the cell. *Curr. Biol.* 9:207–211. https://doi.org/10.1016/S0960-9822(99)80091-8

Klaus, A., and W. Birchmeier. 2008. Wnt signalling and its impact on development and cancer. *Nat. Rev. Cancer.* 8:387–398. https://doi.org/10.1038/nrc2389

Krausova, M., and V. Korinek. 2014. Wnt signaling in adult intestinal stem cells and cancer. *Cell. Signal.* 26:570–579. https://doi.org/10.1016/j.cellsig.2013.11.032

Lee, E.K., and J.A. Diehl. 2014. SCFs in the new millennium. *Oncogene.* 33:2011–2018. https://doi.org/10.1038/onc.2013.144

Li, X.Q., X.L. Yang, G. Zhang, S.P. Wu, X.B. Deng, S.J. Xiao, Q.Z. Liu, K.T. Yao, and G.H. Xiao. 2013. Nuclear β-catenin accumulation is associated with increased expression of Nanog protein and predicts poor prognosis of non-small cell lung cancer. *J. Transl. Med.* 11:114. https://doi.org/10.1186/1479-5876-11-114

Liu, C., Y. Li, M. Semenov, C. Han, G.H. Baeg, Y. Tan, Z. Zhang, X. Lin, and X. He. 2002. Control of beta-catenin phosphorylation/degradation by

a dual-kinase mechanism. *Cell.* 108:837–847. https://doi.org/10.1016/S0092-8674(02)00685-2

Liu, Y.I., M.V. Chang, H.E. Li, S. Barolo, J.L. Chang, T.A. Blauwkamp, and K.M. Cadigan. 2008. The chromatin remodelers ISWI and ACF1 directly repress Wingless transcriptional targets. *Dev. Biol.* 323:41–52. https://doi.org/10.1016/j.ydbio.2008.08.011

Megy, S., G. Bertho, J. Gharbi-Benarous, F. Baleux, R. Benarous, and J.P. Girault. 2005. Solution structure of a peptide derived from the oncogenic protein beta-Catenin in its phosphorylated and nonphosphorylated states. *Peptides.* 26:227–241. https://doi.org/10.1016/j.peptides.2004.09.021

Morin, P.J., A.B. Sparks, V. Korinek, N. Barker, H. Clevers, B. Vogelstein, and K.W. Kinzler. 1997. Activation of beta-catenin-Tcf signaling in colon cancer by mutations in beta-catenin or APC. *Science.* 275:1787–1790. https://doi.org/10.1126/science.275.5307.1787

Pai, L.M., S. Orsulic, A. Bejsovec, and M. Peifer. 1997. Negative regulation of Armadillo, a Wingless effector in Drosophila. *Development.* 124:2255–2266.

Parks, S.K., and J. Pouyssegur. 2015. The Na(+)/HCO3(-) Co-Transporter SLC4A4 Plays a Role in Growth and Migration of Colon and Breast Cancer Cells. *J. Cell. Physiol.* 230:1954–1963. https://doi.org/10.1002/jcp.24930

Peifer, M. 1993. The product of the Drosophila segment polarity gene armadillo is part of a multi-protein complex resembling the vertebrate adherens junction. *J. Cell Sci.* 105:993–1000.

Peifer, M., and P. Polakis. 2000. Wnt signaling in oncogenesis and embryogenesis--a look outside the nucleus. *Science.* 287:1606–1609. https://doi.org/10.1126/science.287.5458.1606

Petherick, K.J., A.C. Williams, J.D. Lane, P. Ordóñez-Morán, J. Huelsken, T.J. Collard, H.J. Smartt, J. Batson, K. Malik, C. Paraskeva, and A. Greenhough. 2013. Autolysosomal β-catenin degradation regulates Wnt-autophagy-p62 crosstalk. *EMBO J.* 32:1903–1916. https://doi.org/10.1038/emboj.2013.123

Pronobis, M.I., N.M. Rusan, and M. Peifer. 2015. A novel GSK3-regulated APC:Axin interaction regulates Wnt signaling by driving a catalytic cycle of efficient βcatenin destruction. *eLife.* 4:e08022. https://doi.org/10.7554/eLife.08022

Reim, G., M. Hruzova, S. Goetze, and K. Basler. 2014. Protection of armadillo/β-Catenin by armless, a novel positive regulator of wingless signaling. *PLoS Biol.* 12:e1001988. https://doi.org/10.1371/journal.pbio.1001988

Reshkin, S.J., M.R. Greco, and R.A. Cardone. 2014. Role of pHi, and proton transporters in oncogene-driven neoplastic transformation. *Philos. Trans. R. Soc. Lond. B Biol. Sci.* 369:20130100. https://doi.org/10.1098/rstb.2013.0100

Sadot, E., M. Conacci-Sorrell, J. Zhurinsky, D. Shnizer, Z. Lando, D. Zharhary, Z. Kam, A. Ben-Ze'ev, and B. Geiger. 2002. Regulation of S33/S37 phosphorylated beta-catenin in normal and transformed cells. *J. Cell Sci.* 115:2771–2780.

Sahai-Hernandez, P., A. Castanieto, and T.G. Nystul. 2012. Drosophila models of epithelial stem cells and their niches. *Wiley Interdiscip. Rev. Dev. Biol.* 1:447–457. https://doi.org/10.1002/wdev.36

Schönichen, A., B.A. Webb, M.P. Jacobson, and D.L. Barber. 2013. Considering protonation as a posttranslational modification regulating protein structure and function. *Annu. Rev. Biophys.* 42:289–314. https://doi.org/10.1146/annurev-biophys-050511-102349

Sedgwick, A.E., and C. D'Souza-Schorey. 2016. Wnt Signaling in Cell Motility and Invasion: Drawing Parallels between Development and Cancer. *Cancers (Basel).* 8:80. https://doi.org/10.3390/cancers8090080

Shafique, S., S. Younis, H. Niaz, and S. Rashid. 2016. Elucidation, functional clustering and structural characterization of βTrCP1 substrates through a molecular dynamics study. *Mol. Biosyst.* 12:2233–2246. https://doi.org/10.1039/C6MB00189K

Simons, M., W.J. Gault, D. Gotthardt, R. Rohatgi, T.J. Klein, Y. Shao, H.J. Lee, A.L. Wu, Y. Fang, L.M. Satlin, et al. 2009. Electrochemical cues regulate assembly of the Frizzled/Dishevelled complex at the plasma membrane during planar epithelial polarization. *Nat. Cell Biol.* 11:286–294. https://doi.org/10.1038/ncb1836

Stamos, J.L., and W.I. Weis. 2013. The β-catenin destruction complex. *Cold Spring Harb. Perspect. Biol.* 5:a007898. https://doi.org/10.1101/cshperspect.a007898

Stehbens, S., H. Pemble, L. Murrow, and T. Wittmann. 2012. Imaging intracellular protein dynamics by spinning disk confocal microscopy. *Methods Enzymol.* 504:293–313. https://doi.org/10.1016/B978-0-12-391857-4.00015-X

Ulmschneider, B., B.K. Grillo-Hill, M. Benitez, D.R. Azimova, D.L. Barber, and T.G. Nystul. 2016. Increased intracellular pH is necessary for adult epithelial and embryonic stem cell differentiation. *J. Cell Biol.* 215:345–355. https://doi.org/10.1083/jcb.201606042

Valenta, T., G. Hausmann, and K. Basler. 2012. The many faces and functions of β-catenin. *EMBO J.* 31:2714–2736. https://doi.org/10.1038/emboj.2012.150

Waghmare, I., and A. Page-McCaw. 2018. Wnt Signaling in Stem Cell Maintenance and Differentiation in the Drosophila Germarium. *Genes (Basel).* 9:E127.

Webb, B.A., K.A. White, B.K. Grillo-Hill, A. Schönichen, C. Choi, and D.L. Barber. 2016. A Histidine Cluster in the Cytoplasmic Domain of the Na-H Exchanger NHE1 Confers pH-sensitive Phospholipid Binding and Regulates Transporter Activity. *J. Biol. Chem.* 291:24096–24104. https://doi.org/10.1074/jbc.M116.736215

White, K.A., D. Garrido Ruiz, Z.A. Szpiech, N.B. Strauli, R.D. Hernandez, M.P. Jacobson, and D.L. Barber. 2017a. Cancer-associated arginine-to-histidine mutations confer a gain in pH sensing to mutant proteins. Sci. Signal.10:eaam9931. https://doi.org/10.1126/scisignal.aam9931

White, K.A., B.K. Grillo-Hill, and D.L. Barber. 2017b. Cancer cell behaviors mediated by dysregulated pH dynamics at a glance. *J. Cell Sci.* 130:663–669. https://doi.org/10.1242/jcs.195297

Wolff, T. 2000. Histological techniques for the Drosophila eye. Part I: Larva and pupa. *In* Drosophila Protocols. W. Sullivan, M. Ashburner, and R.S. Hawley, editors. Cold Spring Harbor Laboratory Press, Cold Spring Harbor, New York. 201–227.

Wu, G., G. Xu, B.A. Schulman, P.D. Jeffrey, J.W. Harper, and N.P. Pavletich. 2003. Structure of a beta-TrCP1-Skp1-beta-catenin complex: destruction motif binding and lysine specificity of the SCF(beta-TrCP1) ubiquitin ligase. *Mol. Cell.* 11:1445–1456. https://doi.org/10.1016/S1097-2765(03)00234-X